Electric-field-driven hole carriers and superconductivity in diamond

K. Nakamura,[1,*] S. H. Rhim,[2,†] A. Sugiyama,[1] K. Sano,[1] T. Akiyama,[1] T. Ito,[1] M. Weinert,[3] and A. J. Freeman[2]

[1]*Department of Physics Engineering, Mie University, Tsu, Mie 514-8507, Japan*

[2]*Department of Physics and Astronomy, Northwestern University, Evanston, Illinois 60208, USA*

[3]*Department of Physics, University of Wisconsin-Milwaukee, Milwaukee, Wisconsin 53201, USA*

(Received 11 March 2013; published 6 June 2013)

First-principles calculations of electric-field-driven superconductivity at the hydrogenated diamond (110) surface are presented. While the hydrogens on the surface effectively maintain the intrinsic sp^3 covalent nature of diamond, the hole carriers induced by an external negative electric field (E-field) lead to a metallic surface region. Importantly, the concentration of hole carriers, confined within a few carbon layers of thickness ∼5–10 Å below the surface, exceeds 10^{21} cm^{-3}, which is larger than the critical hole density responsible for superconductivity in the boron-doped diamond, while the calculated electron-phonon coupling constants are comparable in magnitude, suggesting the possibility of superconductivity with enhanced critical field.

DOI: 10.1103/PhysRevB.87.214506 PACS number(s): 73.20.At, 73.61.Cw, 74.78.−w

I. INTRODUCTION

Diamond, a prototype for hardness and incompressibility, exhibits typical covalent sp^3 bonding. The possibility of superconductivity has been explored in diamond because of its large phonon frequency of 150 meV, (compared with a few meV in most superconducting metals) in the hope that tuning the electron-phonon coupling, λ, might induce superconductivity.[1,2] This new class of superconductors with directional covalent bonding, most likely electron-phonon mediated, consists not only of doped diamond, but also other doped semiconductors.[3] It was predicted that doping a semiconductor with many-valley features in the band structure would induce an effective interaction to overcome the Coulomb repulsion;[4,5] this mechanism was confirmed in subsequent experiments on reduced $SrTiO_3$[6] and $Ge_{1-x}Te$,[7] albeit with rather low transition temperatures, T_c, of at most 0.5 K. Nevertheless, the discovery[8–10] of superconductivity in boron-doped diamond has excited interest in this new class of superconductors, which now also extends to silicon[11] and SiC.[12,13] In doped diamond, the concentration of B dopants exceeded a critical value responsible for a metal-insulator transition, which eventually induced superconductivity around 7–9 K with carrier densities of $\sim 10^{21}$ cm^{-3}.[8,14]

The pairing mechanism in B-doped diamond is likely to be electron-phonon mediated[15,16]—all *ab initio* calculations, both virtual crystal approximation (VCA)[17–19] and direct supercell calculations,[20–22] conclude that superconductivity is due to softened optical modes near the zone center caused by B doping. The deformation potential is 60% of the corresponding quantity in MgB_2;[17,18,20] the three-dimensional nature of diamond significantly reduces the softening, thereby resulting in a smaller T_c. Although an increase of dopant concentration generally raises T_c in doped diamond, problems associated with structural disorder, including B dimers and interstitials, and the appearance of an impurity band are intrinsically unavoidable,[2,23,24] leading to a reduction in doping efficiency, and hence a suppression of T_c.

An alternative route to achieve doping is by applying an electric field (E-field), which overcomes the aforementioned issues related to chemical doping. Very recently, E-field-driven carrier doping has been successfully demonstrated in $SrTiO_3$, the electric double layer formed by an organic electrolyte interface[25] produces a strong E-field. Moreover, E-field carrier doping with an ionic electrolyte leads to superconductivity in $KTaO_3$,[26] which was not achievable by traditional chemical doping. In diamond, where a hydrogen termination persists even in the presence of electrolytes,[27] the degree of carrier doping is limited by the dielectric breakdown field of ∼0.1–0.2 V/Å. A quantitative prediction of the induced carriers, the screening behavior, and the enhanced critical field in the presence of E-field as a result of the interplay between the electronic structure and induced carriers, is desirable to assess the feasibility of E-field-driven superconductivity in diamond. Furthermore, as the three-dimensional nature in doped diamond suppresses the phonon softening (compared to MgB_2), a quasi-two-dimensional system at the surface/interface of the diamond may be advantageous.

In the present work, the electronic structure of the hydrogenated diamond (110) surface is presented in the presence of an external E-field using first-principles calculations. The diamond (110) surface, unlike the other (111) and (100) surfaces, has no reconstruction even at high annealing temperatures.[28] The hydrogen termination sufficiently restores the bulklike geometry at the surface,[29,30] even in the presence of the E-field. Indeed, our results predict that introducing a negative E-field induces hole carriers confined within a few carbon layers below the surface, resulting in a metallic surface region with accumulated hole carriers exceeding the critical carrier density responsible for superconductivity in B-doped diamond.

II. MODEL AND METHOD

We model the hydrogenated diamond (110) surface with a single slabs of 13 carbon layers, where both sides of the slab are hydrogen terminated, as shown in Fig. 1. The in-plane lattice constants are taken to be those calculated for bulk diamond. All atomic positions are fully optimized using atomic force calculations, including the contributions from the external E-field. We confirmed that calculations using a hydrogen-terminated 17-carbon-layer slab do not alter the results or conclusions discussed below.

Calculations were performed using the full-potential linearized augmented plane-wave (FLAPW) method, which

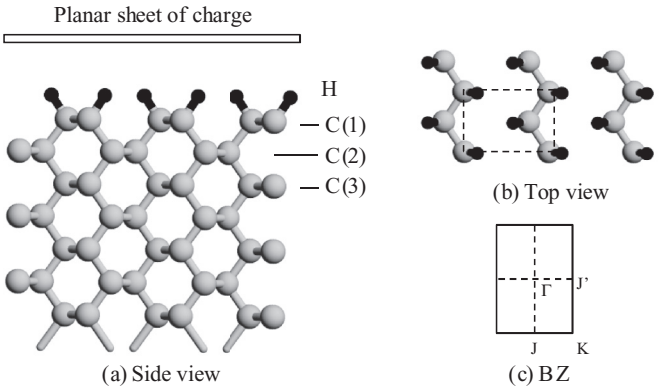

FIG. 1. Atomic structure of the hydrogenated diamond (110) surface, (a) side view and (b) top view. The single slab consists of 13 carbon layers (gray circles) and is terminated by hydrogens (black small circles) on both sides of the slab. (c) Two-dimensional Brillouin zone of the present calculations, corresponding to the unit cell represented by the dotted rectangle in (b).

treats a single slab geometry[31,32] allowing the straightforward inclusion of a uniform E-field along the surface normal.[33,34] We place a planar sheet of charge with surface density $\sigma = q/A$ (q is the charge and A is the area), which generates a normal field $E = 4\pi\sigma\mathbf{n}$; in a vacuum region far enough outside the surface (by 8.8 Å from the position of hydrogen) so that the electrons (i.e., the wave function) at the surface have negligible overlap with the sheet. The requirement of total charge (electrons, nuclei, and sheet) neutrality introduces hole carriers in the slab, which naturally induces a dipole moment of the external and induced densities.[34] With a bulk dielectric constant of 5.6, the applied external E-fields of -1.0 and -0.5 V/Å used in the present calculations are near the maximum expected fields attainable before dielectric breakdown; the calculations themselves for these fields do not exhibit dielectric breakdown.

Self-consistent calculations in the E-field were carried out within the local spin density approximation (LSDA)[35] and the scalar relativistic approximation, i.e., excluding the spin-orbit coupling; LAPW functions with a cutoff of $|\mathbf{k}+\mathbf{G}| \leqslant 5.0$ a.u.$^{-1}$ and muffin-tin (MT) sphere radii of 1.4 and 0.65 a.u. for C and H atoms are used, where the angular momentum expansion inside the MT spheres is truncated at $\ell = 8$ for the wave functions, charge density, and potential. In all, 24×16 special $\mathbf{k}$ points in the two-dimensional Brillouin zone (BZ) were used for the self-consistent calculations.

III. RESULTS AND DISCUSSION

First, we present the atomic and electronic structure of the hydrogenated diamond (110) surface in zero E-field. A small relaxation on the surface is observed; the surface carbons on the C(1) layer move slightly inward, resulting in a shortened bond length of $d_{12} = 1.53$ Å between the first and second carbon layers [C(1)–C(2) in Fig. 1], compared to that in the center of the slab (1.54 Å). The saturation of the dangling bonds with hydrogens, with a H-C(1) bond length of 1.11 Å, recovers almost the bulklike sp^3 bonding geometry even at the surface carbon. The obtained structural parameters in the present calculations agree well with previous theoretical calculations.[36]

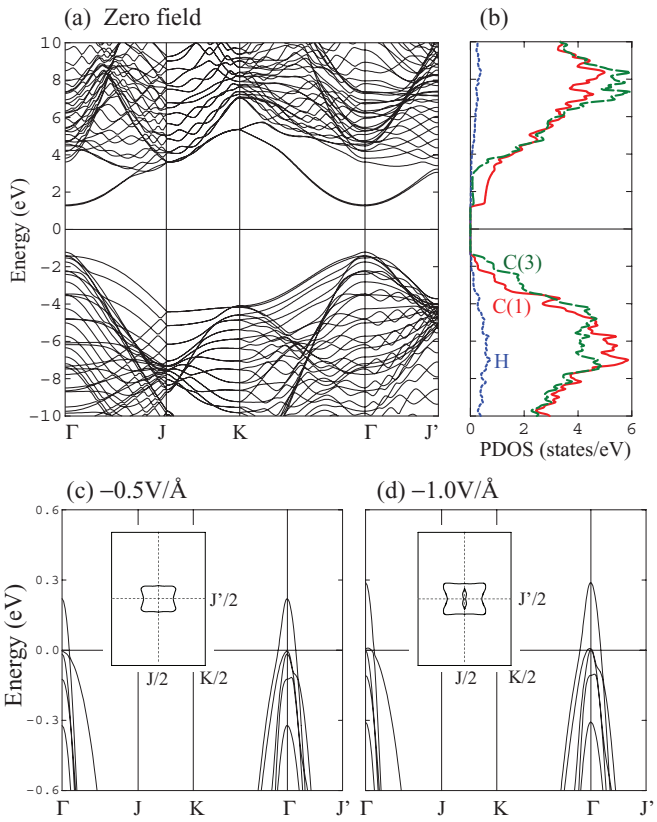

FIG. 2. (Color online) (a) Calculated band structure of the hydrogenated diamond (110) surface in zero E-field. (b) Partial density of states (PDOS) in the carbon muffin-tin spheres at the surface and third layers, [C(1) and C(3)], and the terminating hydrogen (H). Band structures for E-fields of (c) -0.5 V/Å and (d) -1.0 V/Å. In (c) and (d), the reference zero energy is set to the Fermi energy (E_F) located below the top of the valence band at Γ. In the insets, Fermi surfaces with a hole pocket, centered at Γ, are shown in a rectangular zone bounded by J/2 and J'/2.

Figures 2(a) and 2(b) show the calculated band structure in zero E-field along the high-symmetry directions of the BZ as depicted in Fig. 1(c), and the partial density of states (PDOS) in the MT spheres on the surface and the third carbon layers [C(1) and C(3)], and hydrogen (H) atoms. The hydrogen termination removes the dangling bonds that appear in the band gap for the clean surface, and the system becomes semiconducting with a direct gap of 2.48 eV at Γ. An unoccupied surface state of antibonding σ character, lies 1.3 to 5.4 eV above E_F, with a bandwidth of about 4 eV. The valence bands, which consist of the covalent sp^3 bonding-σ states, are almost unchanged compared to the bulk. The PDOS indicates that the contribution to the DOS at the top of the valence band comes mainly from carbons below the subsurface layers. The strong H-C(1) hybridization at the surface pushes the bonding and antibonding states far away in energy from the band gap, and the H PDOS is significantly broadened in the vicinity of the valence and conduction bands.

We now consider the effect of a negative E-field, which induces hole carriers. A small shortening in the bond lengths is observed, where the maximum change appears in carbon layers below the surface [from C(2) to C(4) layers], but with a

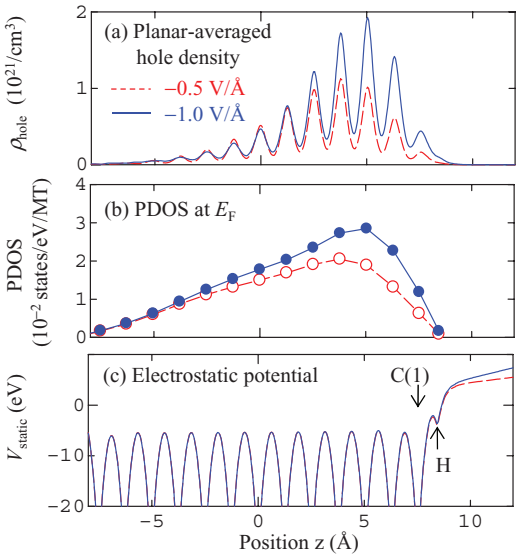

FIG. 3. (Color online) (a) Calculated planar-averaged induced hole density. (b) Partial density of states at E_F in the muffin-tin spheres. (c) Electrostatic potential along the z axis in E-fields of -0.5 (broken line) and -1.0 V/Å (solid line). In (c), arrows indicate the positions of hydrogen (H) and the first carbon layer [C(1)].

magnitude of only 0.003 Å even at -1.0 V/Å. At the surface, there is almost no change in the interatomic distances compared to those in zero E-field. Thus, the E-field does not alter the surface geometry of the diamond (110) surface significantly.

In contrast, as shown in Figs. 2(c) and 2(d), metallicity is induced in the presence of the E-field. The Fermi level is now located below the top of the valence band at Γ, which retains the same structure as in the bulk, showing the validity of the rigid band as seen in the B-doped diamond.[37] When the E-field increases, E_F shifts to lower energy in order to increase the hole density: 2.84×10^{13} and 5.68×10^{13} cm^{-2} for the E-fields of -0.5 and -1.0 V/Å, respectively. A Fermi surface with a hole pocket centered at Γ emerges, as shown in the insets of Figs. 2(c) and 2(d), where the area of the Fermi surface increases when the E-field increases. Interestingly, a nesting feature, characterized by the vector perpendicular to the surface chain, is observed.

Importantly, the E-field-induced hole carriers are confined within a few carbon layers below the surface, which effectively reduces the active dimensionality to two dimensions. This is demonstrated by the planar-averaged hole density—corresponding to states in the energy range from E_F to the valence band maximum—along the z axis as shown in Fig. 3(a). The hole carriers are confined within ∼5–10 Å of the surface, which is much smaller, by a factor of ∼2–4, than that predicted by a one-dimensional model calculation using a Schrödinger-Poisson solver.[27] The PDOS at E_F [Fig. 3(b)] exhibits a similar tendency as the hole density distribution, with the maximum occurring around the C(3) and C(4) layers. The internal E-field inside the slab vanishes, as seen in Fig. 3(c), indicating a screening of the external E-field by the induced holes.

The average hole densities in the MT spheres on the C(3) and C(4) layers are 1.12×10^{21} and 1.32×10^{21} cm^{-3} for the $E = -0.5$ V/Å, and 2.33×10^{21} and 2.08×10^{21} cm^{-3} for $E = -1.0$ V/Å. Thus, the accumulated hole carriers within a few carbon layers below the subsurface exceed the critical carrier density, 10^{21} cm^{-3}, necessary for superconductivity in B-doped diamond.[14] The recent Hall effect measurement[14] clearly demonstrated the T_c dependence on the carrier density. Assuming that the carrier density in our system corresponds to the average hole density, then T_c would correspond to 3 and 4 K for fields of -0.5 and -1.0 eV/Å, respectively.

To make further connections to the conventional electron-phonon superconductivity, we consider the electron-phonon coupling constant, λ, both for the (110) surface in the presence of the E-field and for the B-doped bulk. To estimate λ, the rigid-muffin-tin approximation (RMTA) is used:[38–40] $\lambda = \frac{N(E_F)\langle I^2\rangle}{M\omega^2}$, where $\langle I^2\rangle$, M, ω, are the average electron-phonon interaction matrix, the atomic mass, and vibration frequency, respectively. We estimate λ to be 0.18 and 0.47 for E-fields of -0.5 and -1.0 eV/Å, respectively. For comparison, the RMTA calculations for B-doped diamond give $\lambda = 0.51$ for 12.5% concentration, which agrees well with that obtained in a previous supercell calculation.[18] Thus, within the RMTA, the E-field-induced superconductivity at the (110) surface may be possible.

We note that the thickness (d) of region containing the localized the induced holes of 5∼5–10Å is much smaller than the coherence length (ξ) of the B-doped diamond, ∼100–150Å.[8,9] The system is an intrinsically *clean* superconductor, in contrast to B-doped diamond, and in this thin film limit, $d \ll \xi$, we estimate the Landau (depairing) critical velocity, $v_c = \frac{\Delta}{p_F} = \frac{\hbar}{\pi m \xi} \approx 2.5 \sim 3.5 \times 10^5$ cm/s, which is an order of magnitude larger than those found in conventional superconductors such as Al, Pb, and Nb.[41] Furthermore, for a type-II superconductor with $d \ll \xi$, the critical field (H_{c2}) is modified: the parallel component of the critical field becomes $H_{c2\parallel} = \frac{5.53}{2\pi\xi}\frac{\phi_0}{d}$, where ϕ_0 is the flux quantum,[42] whereas the normal component $H_{c2\perp} = 7T$ does not change. $H_{c2\parallel}$ can be more precisely estimated taking the Pauli paramagnetic limit into account, $\mu_B H_{c2\parallel} = k_B T_C \ \mathcal{U}(\frac{T}{T_C})$, where $\mathcal{U}(x)$ is the universal function in Pauli limiting theory.[41,42] From the asymptotic form of $\mathcal{U}(x) \sim 1.76$ as $x = T/T_c \to 0$ and $\mathcal{U}(x) \sim \frac{\pi}{8}(1-x)$ as $x \to 1$, we estimate the enhanced parallel component of the critical field at $T = 0$ K and near T_C, as $H_{c2\parallel}(0) = 187$ T and $H_{c2\parallel}(T_C) = 41.8$ T, respectively.[43]

IV. SUMMARY

We investigated the band structure of the hydrogenated diamond (110) surface using first-principles calculations, and demonstrated that E-field-driven hole carriers potentially exceed the critical concentrations necessary for superconductivity in the B-doped diamond. The H termination restores the bulklike geometry at the surface, and the intrinsic valence band structure of bulk diamond is effectively preserved even in the presence of the E-field. The negative E-field induces hole carriers, leading to a metallic surface region with E_F located below the top of the valence band around Γ. The accumulated hole carriers are confined within a few carbon layers below the surface with a thickness of ∼5–10 Å, which reduces the dimensionality. The estimated electron-phonon coupling is comparable to that in B-doped diamond and should

be sufficient to induce superconductivity. The E-field-driven superconductivity is intrinsically clean and in the thin film limit where the $H_{c2\|}$ would be greatly enhanced.

ACKNOWLEDGMENTS

We are grateful to John B. Ketterson for fruitful discussions. Work at Mie University was supported by a Grant-in-Aid for Scientific Research (Grants No. 23540405 and No. 20540334) and Young Researcher Overseas Visits Program for Vitalizing Brain Circulation (R2214) from the Japan Society for the Promotion of Science. Computations were partially performed at ISSP, University of Tokyo. Work at Northwestern University was supported by the US Department of Energy (DE-FG02-05ER45372). Work at University of Wisconsin-Milwaukee was supported by NSF DMR-1105839.

*kohji@phen.mie-u.ac.jp
†sonny@u.northwestern.edu

[1] E. Bustarret, Phys. Status Solidi A **205**, 997 (2008).
[2] X. Blase, E. Bustarret, C. Chapelier, T. Klein, and C. Marcenat, Nature Mater. **8**, 375 (2009).
[3] K. Iakoubovskii, Cent. Eur. J. Phys. **7**, 654 (2009).
[4] M. L. Cohen, Phys. Rev. **134**, A511 (1964).
[5] M. L. Cohen, Rev. Mod. Phys. **36**, 240 (1964).
[6] J. F. Schooley, W. R. Hosler, and M. L. Cohen, Phys. Rev. Lett. **12**, 474 (1964).
[7] R. A. Hein, J. W. Gibson, R. Mazelsky, R. C. Miller, and J. K. Hulm, Phys. Rev. Lett. **12**, 320 (1964).
[8] E. A. Ekimov, V. A. Sidrov, E. D. Bauer, N. N. Mel'nik, N. J. Curro, J. D. Thompson, and S. M. Stishov, Nature (London) **428**, 542 (2004).
[9] Y. Takano, M. Nagao, I. Sakaguhci, M. Tachiki, T. Hatano, K. Kobayashi, H. Umezawa, and H. Kawarada, Appl. Phys. Lett. **85**, 2851 (2004).
[10] E. Bustarret, J. Kacmarcik, C. Marcenat, E. Gheeraert, C. Cytermann, J. Marcus, and T. Klein, Phys. Rev. Lett. **93**, 237005 (2004).
[11] E. Bustarret, C. Marcenat, P. Achatz1, J. Kamarik1, F. Levy, A. Huxley, L. Ortega, E. Bourgeois, X. Blase, D. Debarre, and J. Boulmer, Nature (London) **444**, 465 (2006).
[12] Z. A. Ren, J. Kato, T. Muranaka, J. Akimitsu, M. Kriener, and Y. Maeno, J. Phys. Soc. Jpn **76**, 103710 (2007).
[13] M. Kriener, Y. Maeno, T. Oguchi, Z. A. Ren, J. Kato, T. Muranaka, and J. Akimitsu, Phys. Rev. B **78**, 024517 (2008).
[14] A. Kawano, H. Ishiwata, S. Iriyama, R. Okada, T. Yamaguchi, Y. Takano, and H. Kawarada, Phys. Rev. B **82**, 085318 (2010).
[15] J. Bardeen, L. N. Cooper, and J. R. Schrieffer, Phys. Rev. **108**, 1175 (1957).
[16] W. L. McMillan, Phys. Rev. **167**, 331 (1968).
[17] L. Boeri, J. Kortus, and O. K. Andersen, Phys. Rev. Lett. **93**, 237002 (2004).
[18] K. W. Lee and W. E. Pickett, Phys. Rev. Lett. **93**, 237003 (2004).
[19] Y. Ma, J. S. Tse, T. Cui, D. D. Klug, L. Zhang, Yu Xie, Y. Niu, and G. Zou, Phys. Rev. B **72**, 014306 (2005).
[20] X. Blase, Ch. Adessi, and D. Connetable, Phys. Rev. Lett. **93**, 237004 (2004).
[21] H. J. Xiang, Z. Y. Li, J. L. Yang, J. G. Hou, and Q. S. Zhu, Phys. Rev. B **70**, 212504 (2004).
[22] F. Giustino, J. R. Yates, I. Souza, M. L. Cohen, and S. G. Louie, Phys. Rev. Lett. **98**, 047005 (2007).
[23] E. Bourgeois, E. Bustarret, P. Achatz, F. Omnès, and X. Blase, Phys. Rev. B **74**, 094509 (2006).
[24] J. P. Goss and P. R. Briddon, Phys. Rev. B **73**, 085204 (2006).
[25] K. Ueno, S. Nakamura, H. Shiotani, A. Ohtomo, N. Kimura, T. Nojima, H. Aoki, Y. Iwasa, and M. Kawasaki, Nature Mater. **7**, 855 (2008).
[26] K. Ueno, S. Nakamura, H. Shimotani, H. T. Yuan, N. Kimura, T. Nojima, H. Aoki, Y. Iwasa, and M. Kawasaki, Nature Nanotech. **6**, 408 (2011).
[27] M. Dankerl, A. Lippert, S. Birner, E. U. Stutzel, M. Stutzmann, and J. A. Garrido, Phys. Rev. Lett. **106**, 196103 (2011).
[28] P. G. Lurie and J. M. Wilson, Surf. Sci. **65**, 453 (1977).
[29] S. V. Pepper, J. Vac. Sci. Technol. **20**, 213 (1982).
[30] M. McGonigal, J. N. RussellJr., P. E. Pehrsson, H. G. Maguire, and J. E. Butler, J. Appl. Phys. **77**, 4049 (1995).
[31] E. Wimmer, H. Krakauer, M. Weinert, and A. J. Freeman, Phys. Rev. B **24**, 864 (1981).
[32] M. Weinert, E. Wimmer, and A. J. Freeman, Phys. Rev. B **26**, 4571 (1982).
[33] K. Nakamura, R. Shimabukuro, Y. Fujiwara, T. Akiyama, T. Ito, and A. J. Freeman, Phys. Rev. Lett. **102**, 187201 (2009).
[34] M. Weinert, G. Schneider, R. Podloucky, and J. Redinger, J. Phys.: Condens. Matter **21**, 084201 (2009).
[35] U. von Barth and L. Hedin, J. Phys. C **5**, 1629 (1972).
[36] G. Kern and J. Hafner, Phys. Rev. B **56**, 4203 (1997).
[37] T. Yokoya, T. Nakamura, T. Matsushita, T. Muro, Y. Takano, M. Nagao, T. Takenouchi, H. Kawarada, and T. Oguchi, Nature (London) **438**, 647 (2005).
[38] G. Gaspari and B. Gyorffy, Phys. Rev. Lett. **28**, 801 (1972).
[39] H. L. Skriver and I. Mertig, Phys. Rev. B **41**, 6553 (1990).
[40] S. H. Rhim, R. Saniz, J. Yu, L. H. Ye, and A. J. Freeman, Phys. Rev. B **76**, 184505 (2007).
[41] P.-G. de Gennes, *Superconductivity of Metals and Alloys* (Addison-Wesley, Boston, 1966).
[42] J. B. Ketterson and S. N. Song, *Superconductivity* (Cambridge University Press, Cambridge, 1999).
[43] Experimental values of ξ and H_{c2} are taken from Ref. 9. With H_{c2} and T_C from Ref. 8, $H_{c2\|}(0)$ and $H_{c2\|}(T_C)$ are estimated as 101 and 22 T, respectively.